Relations between fragmentation, plastic work and critical state in crushable rock clasts

Wei HU [1], Zhen-Yu YIN [2]*, Gianvito SCARINGI [1],

Christophe DANO [3], and Pierre-Yves HICHER [2]

[1] State Key Laboratory of Geohazard Prevention and Geoenvironment Protection, Chengdu University of Technology, Chengdu, 610059, China.

[2] Research Institute in Civil and Mechanical Engineering, Ecole Centrale de Nantes, Nantes, UMR CNRS 6183, France

[3] Laboratoire 3SR Domaine Universitaire, Grenoble Cedex 9, BP5338041, France

[*] Corresponding to Dr. Zhen-Yu YIN, zhenyu.yin@gmail.com

ABSTRACT

Extensive clasts fragmentation during the runout of rock and debris avalanches has been recognized as one important mechanism responsible for the avalanches' catastrophic behavior. Here we present results of laboratory tests on limestone fragments under various stress paths, and we investigate the relationship between the progression of grain breakage, the plastic work and the evolution of the critical state line, that controls the grains' mechanical behavior. Using the plastic work concept, we propose a method for determining grain shape and grain breakage indices, and we show how grain breakage influences the critical stress state, and hence the mechanical behavior. The validity of the relationships is verified on various crushable granular materials with different mineralogy. Finally, an engineering chart is proposed to characterize the evolution of grain breakage and critical state according to the grains' mineral composition.

Keywords: particle crushing; fragmentation; rock avalanche; critical state; mineralogy

1. INTRODUCTION

Rock avalanches are among the most deadly and destructive types of landslides because of their high speed and long runout distance (Evans et al., 2007; Deganutti, 2008; Xu et al., 2012; Hungr et al., 2014; Robinson et al., 2015; Dai et al., 2016; Zhang et al., 2016a; Zhang and McSaveney, 2017). They are often triggered by large earthquakes or extreme rainfall events (Van Asch et al., 1999; Gorum et al., 2011; Huang et al., 2012; Fan et al., 2017), and can cause extensive property and infrastructure damage, and loss of human lives (Nadim et al., 2006; Keefer and Larsen, 2007; Petley, 2012).

Davies et al. (1999) first suggested that the extraordinarily long runout of large rock avalanches may result from the continuing fragmentation of clasts through the fall and runout. Some studies argue that fragmentation may not be the (main) cause of the long-runout (Deganutti, 2008; Kaproth et al., 2010; Lucas et al., 2014; Johnson et al., 2015; Wang et al., 2015, 2017; Scaringi et al., 2017; Hu et al., 2018), and the issue is nowadays still debated (Davies and McSaveney, 2016; Wang et al., 2017). Nonetheless, the widespread presence of fragmented material in the avalanche deposits and their morphology support the fragmentation hypothesis, and so do several simulations and laboratory experiments (Davies and McSaveney, 2002; Locat et al., 2006; McSaveney and Davies, 2006; Crosta et al., 2007; Taboada and Estrada, 2009; Imre et al., 2010; Bowman et al., 2012; McSaveney, 2015; De Blasio and Crosta, 2015; Jiang et al., 2016; Dufresne and Dunning, 2017; Zhao et al., 2017).

Furthermore, a correct evaluation of the post-runout physical and mechanical properties of deposits of rock clasts residing on hillslopes and in drainage channels (such as those generated by the 2008 M_w 7.9 Wenchuan Earthquake in Sichuan, China; Gorum et al., 2011; Huang and Fan, 2013; Zhang et al., 2016b) is crucial for understanding their likelihood to exhibit instability, collapse, liquefaction, and to move again with catastrophic effects due to seismic shaking or strong hydrological events (Koi et al., 2008; Tang et al., 2012; Xu et al., 2012; Hu et al., 2015, 2017a, 2017b).

Clasts fragmentation (also termed grain breakage) may occur during compression and

shearing, especially under high confining stresses and dynamic loadings (Harireche and McDowell, 2003; McDowell and Lu, 2010; Kaproth et al., 2010; Coop and Altuhafi, 2011; Kimura et al., 2014; Liu et al., 2017; Zhang and McSaveney, 2017). The amount of fragmentation can be quantified from the change of grain size distribution (GSD). Different measures of its evolution have been proposed (Lee and Farhoomand, 1967; Marsal, 1967; Hardin, 1985; Lade et al., 1996; Nakata et al., 1999; Einav, 2007). The influence of grain breakage on various physical and mechanical properties has been investigated (Miura et al., 1984; McDowell et al., 1996; Biarez and Hicher, 1997; McDowell and Bolton, 1998; Cheng et al., 2003; Coop et al., 2004; Indraratna et al., 2009; Bandini and Coop, 2011; Miao and Airey, 2013; Zhang and Baudet, 2013, 2014), and introduced into constitutive and numerical modelling (Simonini, 1996; Daouadji et al., 2001; Cecconi et al., 2002; Russell and Khalili, 2004; Yao et al., 2008; Kikumoto et al., 2010; Ma et al., 2017; Zhou, 2017). However, how the breakage amount can be measured and how this measure can be correlated with mechanical properties explicitly are still a challenge. The three following issues need to be investigated: (1) what are suitable measures for the amount of grain breakage; (2) how to determine these measures based on stress-strain histories; and (3) how to relate these measures to mechanical properties of the granular assembly. Once these three points are solved, the quantity measuring the amount of grain breakage can be introduced as a variable to control the influence of grain breakage on the mechanical properties of a granular material subjected to a generic stress-strain history.

For the first issue, a breakage measure varying from zero to one with the changes of GSD might be convenient. Among the proposed measures, the modified relative breakage index B_r^* of Einav (2007), and the relative uniformity B_u, based on the fractality of the GSD (McDowell and Bolton, 1998; Cheng et al., 2003; Coop et al., 2004) and on the coefficient of uniformity C_u, seem good choices. Various methods to quantify the GSD change under different loading conditions were developed and validated through tests under monotonic loading: i.e. the crushing surface approach by Simonini (1996) and Kikumoto et al. (2010), and the energy approach by Lade et al. (1996) and Einav (2007). So far, these two approaches haven’t been fully examined

under different loading conditions, including under cyclic loading. Therefore, in this paper we propose a unified approach to quantify the change of GSD (in terms of B_u and B_r^*) for different loading conditions.

As fragmentation can influence the mechanical behavior of crushable granular materials significantly, the GSD change can be correlated to the evolution of mechanical properties. Several properties (stress-dilatancy, peak shear strength, plastic modulus, etc.) depend on the distance between the current stress state (p', e) and the corresponding critical state (p', e_c) of the granular material (Wroth and Bassett, 1965; Been and Jefferies, 1985). Hence, how fragmentation-induced changes of GSD affect the location of the critical state line (CSL) is crucial for quantifying the influence of grain breakage on mechanical properties. The CSL-GSD relationship has been demonstrated by experiments on crushable sands (Biarez and Hicher, 1997; Bandini and Coop, 2011) and by discrete element simulations on crushable granular materials (Bolton et al., 2008). This idea is also supported by experimental results showing the evolution of the CSL with grading on sand with various fine contents (Thevanayagam et al., 2002) and by numerical results on granular materials with different GSDs by means of discrete element simulations (Kikumoto et al., 2010; Muir Wood and Maeda, 2007). Therefore, the third task of this paper is to propose a relation between the evolution of the CSL location and the breakage measures (B_u and B_r^*) during loading.

We first investigate the measures of grain breakage amount. Laboratory tests on crushable limestone grain assembly with various stress strain paths under both monotonic and cyclic loadings were carried out to propose a unified determination method for the measure of grain breakage. Secondly, the test results are also used to propose a relation between these measures and the CSL location. Finally, the relations obtained on limestone grain material are applied on other materials with different mineral contents for the validation of the method.

2. MEASURE OF GRAIN BREAKAGE AMOUNT

Different measures have been proposed in the literature, such as: (1) $\mathbf{B_{15}=D_{15i}/D_{15f}}$, where D_{15} is the grain diameter for a percentage of passing equal to 15% in weight, and subscript "i" and

"f" represent the samples before and after testing, respectively, as proposed by Lee and Farhoomand (1967), shown in Fig. 1(a); (2) **R/100:** increase in percent passing the sieve having the greatest increase, measured from the grading curves before and after testing by Marsal (1967), shown in Fig. 1(b); (3) the relative breakage $\mathbf{B_r=B_t/B_p}$: B_p is the area between the line defining the upper limit of the silt size d=0.074 mm and the part of the initial grading curve for which d > 0.074 mm, and B_t is the area between the part of the initial grading curve (the initial grading means the natural grading of the granular materiel before loading) and the part of the grading curve after loading for which d > 0.074 mm) by Hardin (1985), shown in Fig. 1(c); (4) the particle breakage factor $\mathbf{B_{10}=1- D_{10f}/D_{10i}}$ by Lade et al. (1996), shown in Fig. 1(d); (5) the change of the uniformity coefficient $\mathbf{C_u=D_{60}/D_{10}}$ related to the amount of grain breakage by Biarez and Hicher (1997). shown in Fig. 1(e); (6) the simple particle breakage factor $\mathbf{B_f=R/100}$ where *R* is the percentage of particles smaller, after testing, than the minimum particle size in the initial grading curve by Nakata et al. (1999), shown in Fig. 1(f); (7) the modified relative breakage index $\mathbf{B_r^*=B_t/B_p}$, obtained by replacing the cut-off line of silt particle size by an ultimate GSD in the definition of Hardin's B_p and B_t, proposed by Einav (2007), shown in Fig. 1(g); (8) the grading state index $\boldsymbol{I_G=B_t/B_p}$ with the initial grading curve determined by lower limit of the biggest particle size by Kikumoto et al. (2010). Note that I_G has an initial value for samples without uniform particle size, shown in Fig. 1(h).

Since the GSD tends to approach a fractal distribution according to compression tests by McDowell and Bolton (1998) and shear tests by Coop et al. (2004), only the breakage measure B_r^* by Einav (2007) varies from zero to one with changes in GSD. This particular aspect might be convenient in practice. Therefore, the modified relative breakage index B_r^* should be a good choice to describe the breakage amount.

Another possible way is to define another coefficient, called the relative uniformity B_u, based on the uniformity coefficient $C_u=D_{60}/D_{10}$ which varies with grain breakage, as follows

$$B_u = \frac{C_u - C_{ui}}{C_{uf} - C_{ui}} \tag{1}$$

where C_{ui} represents the initial uniformity coefficient; and C_{uf} represents the ultimate uniformity

coefficient corresponding to the fractal GSD. Thus, B_u varies also from zero to one. Note that B_u includes also the change of D_{10} which is a factor influencing the mechanical properties as pointed out by Lade et al. (1996). Since the definition of B_u is based on C_u which is a common coefficient in engineering practice and can be easily measured, the use of B_u is convenient from a practical point of view to describe the grain breakage amount, provided that it can be related to mechanical variables influencing grain breakage. Therefore, in addition to B^*_r, B_u is also examined in this study in connection with the amount of grain breakage.

3. UNIFIED APPROACH IN DETERMINING GRAIN BREAKAGE AMOUNT

As grain breakage is produced by mechanical loading, the breakage amount can be related to the input energy. Based on this idea, Lade et al. (1996) proposed a hyperbolic relation between the particle breakage factor B_{10} and the total energy input calculated by stresses and total strains. Einav (2007) proposed to link the breakage energy, using stresses and total strains, with the relative breakage B_r^* for compression tests. Different from the energy methods, Simonini (1996) and Kikumoto et al. (2010) defined a crushing surface to determine the breakage amount based on the distance between the stress state and this crushing surface. However, the accumulation of grain breakage during cyclic loading cannot be described by these different approaches.

Another possible variable related to the breakage amount can be the plastic work as proposed by Daouadji et al. (2001). To avoid the non-uniqueness of the summation of the plastic work along a loading path where stresses or strains are reversed, we adopted the following classical definition of the plastic work, differently from Daouadji et al. (2001):

$$w_p = \int \left\langle \sum \sigma d\varepsilon^p \right\rangle \tag{2}$$

where σ and $d\varepsilon^p$ are stress and incremental plastic strain tensors, respectively, and the use of Macaulay's brackets implies that $\langle F \rangle = \left(|F| + F\right)/2$. Using the Eq. (2), the plastic work can be accumulated during cyclic loading. Thus, linking the plastic work to the measure of breakage amount makes it possible to take the additional grain breakage after the first loading into account.

In order to establish the relationship between the breakage measures (B_u and B_r^*) and the

plastic work, drained triaxial tests under both monotonic and cyclic loadings on crushable limestone grain assemblies were carried out. For each test, the GSD was measured after testing and the plastic work was calculated along the loading path.

3.1. PHYSICAL AND MECHANICAL PROPERTIES OF TESTED MATERIAL

The tested material is an assembly of limestone grains from a quarry located in Prefontaines, in the center of France. This material is often used for the construction of small embankments and is very crushable. The shape of the particles is classified as sub-angular according to the ASTM D2488-10 standard. The unit weight of the material is 17.1 kN/m^3 and the specific weight is 2.70 g/cm^3. The prepared samples have an initial uniformity coefficient C_u = 1.8. The mean grain size is D_{50} = 6 mm. The minimum grain size d_m is 1 mm and the maximum grain size d_M is 10 mm. The maximum and minimum void ratios are 1.43 and 0.83, respectively. The initial void ratio e_0 for all tested samples varies from 1.05 to 1.1. All samples have a diameter of 70 mm and a height of 105 mm. The rate of axial displacement for all triaxial tests was 0.03 mm/min. All samples were saturated before testing. The correction of the cross section and the correction of membrane penetration are considered by applying the French Standard NF P 94-074 and the method of Head (1992).

Fig. 2 shows the photographs of the material before testing and after a drained triaxial test under a constant mean effective stress p' = 400 kPa. Comparing Fig. 2(b) and Fig. 2(a), one can see that some grains were crushed into smaller pieces, and some grains were damaged with visible cracks, while some others appear still intact. The breakage amount can be estimated by the GSD measured after testing.

Fig. 3a presents the results of two conventional drained triaxial tests with confining stresses p'_0 = 50 and 100 kPa. The elastic properties can be measured on the stress-strain curves. We assume a non-linear elasticity and we adopt the formulation proposed by Richart et al. (1970),

$$G = G_0 p_{at} \frac{(2.97 - e)^2}{1 + e} \left(\frac{p'}{p_{at}} \right)^{0.5} \quad (3)$$

$$K = K_0 p_{at} \frac{(2.97-e)^2}{1+e} \left(\frac{p'}{p_{at}} \right)^{0.5} \quad (4)$$

where p_{at} = 101.325 kPa is the atmosphere pressure; e is the void ratio.

The shear modulus was measured on the stress-strain curves up to a deviatoric strain of 0.1% in Fig. 3(a). We found G_0 = 80. The bulk modulus was measured from the isotropic compression tests (Fig. 3b). We found K_0 = 105 which corresponds to a Poisson's ratio of 0.2. Taking into consideration the decrease of the shear modulus with the strain level for various sands (Hicher, 1996; Jovicic and Coop, 1997; Clayton, 2010), we can assume that the elastic modulus at very small strain is approximately five times bigger than the elastic modulus at 0.1%. Therefore, G_0 = 400 and K_0 = 525 corresponding to the very small strain level were used hereafter on to estimate the elastic strain component.

3.2. TESTS UNDER MONOTONIC LOADING

According to McDowell et al. (1996), the grading curve for both initial and tested samples can be approximately expressed as follows

$$F(D) = \left(D / d_M \right)^{3-\alpha} \quad (5)$$

where $F(D)$ is the percentage of passing corresponding to the grain size D. In agreement with Einav (2007), a fractal GSD was assumed with α = 2.6 according to Coop et al. (2004). Therefore, the relative breakage index B_r^* for each test can be obtained as proposed by Einav (2007).

For the measure of B_u, the current C_u and the ultimate C_{uf} are needed besides C_{ui}. C_u can be obtained from the grading curve at the end of each test. C_{uf} corresponding to fractal GSD can be determined using Eq. (5) with α = 2.6 as follows: for $F(D)$ = 60% and 10%, $60\% = (D_{60}/d_M)^{3-2.6}$ and $10\% = (D_{10}/d_M)^{3-2.6}$, then $C_{uf} = D_{60}/D_{10} = 6^{1/(3-2.6)} = 88.18$ is obtained. Therefore, based on Eq. (1), the value of B_u can be obtained once C_u is measured at the end of each test.

3.2.1. Tests at different confining stresses

Drained triaxial tests under different constant confining stresses (constant-σ'_3 tests) varying from 22 kPa to 800 kPa were carried out (see Fig. 4). One can notice that, for elevated confining

stresses, the material appears very ductile and the stress ratio q/p' continues to increase even at large strains (Fig 4a). This is due to a large amount of particle breakage developing during loading as shown in Fig. 4(c).

Fig. 4(b) presents the volume changes during the drained triaxial tests. They show a dilative behaviour under low confining stresses of 22 kPa and 50 kPa, and a contractive behaviour under higher confining stresses of 100 kPa, 400 kPa and 800 kPa. For samples under high confining stresses, the large contraction is also a consequence of a significant grain breakage.

The GSDs after testing were measured, as shown in Fig. 4(c). The tested material is very crushable, even under low confining stresses. The relative uniformity B_u and the modified relative breakage index B_r^* were then obtained for each test, and the values summarized in this figure. The results show that a higher confining stress induces a higher amount of grain breakage, thus raises the values of B_u and B_r^*.

3.2.2. Tests with different loading paths

A drained triaxial test under a constant mean effective stress (constant-p' test) p' = 400 kPa up to ε_a = 25 % was carried out, as shown in Fig. 5. The results are compared to the constant-σ'_3 test results at the same consolidation stress. During the constant-p' test, the lateral stress is reduced in order to keep p' constant, which also results in a smaller amplitude of the deviatoric stress. As a consequence, less grain breakage occurred compared to the constant-σ'_3 test (Fig. 5c). This leads to a stiffer stress-strain relationship and a smaller volume change for the constant-p' test. The evolution of the stress-strain relationship with the grading change is similar to the one obtained for the previous constant-σ'_3 tests. Note that the variability of the grading measurements for a given stress history is mainly due to the amount of fine particles (e.g. < 2 mm). In Fig. 5c, the difference in the gradation curves between the constant p' and the constant σ'_3 tests is statistically significant, especially for particles bigger than 2 mm.

The values of B_u and B_r^* for the constant-p' test are smaller than those for the constant-σ'_3 test.

3.2.3. Tests with different consolidation histories

A conventional drained triaxial test at σ'_3 = 100 kPa up to ε_a = 25 % on a sample isotropically consolidated up to 800 kPa and unloaded to 100 kPa was carried out, and compared to the constant-σ'_3 test with σ'_3 = 100 kPa without an over-consolidation history (see Fig. 6). Although the whole difference of grading between the two tests is small (see Fig. 6c), the difference of distribution for particles bigger than 2 mm was adequately measured. The results show the influence of the stress history on the grain breakage: the test with the over-consolidation process results in slightly more grain breakage than the test without the over-consolidation history (B_u and B_r^* for the former are higher than for the latter). This is essentially due to the isotropic loading phase up to 800 kPa where plastic strains developed (see Fig. 3b). The shearing phase did not bring any significant additional grain breakage and, therefore, the stress-strain relationship and the volume change for these two tests are in agreement with what is usually observed by comparing normally and over-consolidated material behaviours: a stiffer and less contractive behaviour for the over-consolidated sample.

3.3. CYCLIC LOADING TESTS

In order to seek a unified approach for determining the breakage amount under different loading conditions, three types of drained cyclic triaxial tests on samples isotropically consolidated at 400 kPa were carried out:

- **Series 1:** two tests with constant confining stress, CYC-CCS1 in which q_{max} and q_{min} increase from one cycle to another, CYC-CCS2 with constant q_{max} and q_{min}, in order to investigate the influence of the axial loading amplitude on grain breakage;
- **Series 2:** three tests under constant p' with different number of cycles N_{cycle} = 0, 5, 20 (CYC-CP0, CYC-CP5 and CYC-CP20) to investigate the influence of the number of cycles on grain breakage;
- **Series 3:** a test with constant deviatoric stress with varying p' (CYC-CDS) to investigate the influence of the stress ratio on grain breakage.

3.3.1. Tests at constant confining stress

Fig. 7 shows the stress-strain curves and GSDs for two tests at constant confining stress (**Series 1**). The test CYC-CCS1 was strain-controlled with axial strains up to 1%, -1%, 2%, -2%, 3%, -3%, 4%, and ending by -4%. q_{max} reached 370, 570, 770 and 890 kPa, and q_{min} reaches to -250, -310, -310, -310 kPa. The test CYC-CCS2 was stress-controlled with the axial stress varying between q_{max} = 865 kPa and q_{min} = -310 kPa for 4 cycles. The stress-strain curves in Fig. 7(a) and the evolution of the volumetric strain in Fig. 7(b) can be used to calculate the plastic work during the tests. The amount of grain breakage in Test CYC-CCS1 is lower than the one in Test CYC-CCS2 (Fig. 7c), because the values of q_{max} during the first three cycles for Test CYC-CCS1 are smaller than those applied in Test CYC-CCS2 (Fig. 7a).

3.3.2. Tests with constant mean effective stress

Fig. 8 shows the GSDs for tests at constant *p'* with different number of cycles (**Series 2**). For the test CYC-CP0, the sample was only monotonically sheared up to q = 730 kPa with ε_a = 10 % and q/p' = 1.83. The other two tests CYC-CP5 and CYC-CP20 were carried out with q_{max} = 730 kPa and q_{min} = -420 kPa (q/p' between 1.83 to -1.05) up to 5 and 20 cycles, respectively. The stress-strain curves in Fig. 8(a) and the evolution of the volumetric strains in Fig. 8(b) can be used to calculate the plastic work. The amount of grain breakage observed after testing increases with the applied number of cycles (Fig. 8c). Fig. 8(d) shows the evolution of B_u and B_r^* with the number of cycles N_{cycle}, which demonstrates that the grain breakage occurs very fast at the beginning of the loading, and then slows down. Based on this figure, the evolution of these two variables can be expressed by

$$\mathrm{B}_u = B_{u0} + \frac{\left(B_{u\max} - B_{u0}\right) N_{cycle}}{a + N_{cycle}} \;\; ; \quad B_r^* = B_{r0}^* + \frac{\left(B_{r\max}^* - B_{r0}^*\right) N_{cycle}}{b + N_{cycle}} \tag{6}$$

with B^*_{r0} = 0.065, B^*_{rmax} = 0.215, a = 4; and B_{u0} = 0.0054, B_{umax} = 0.037, b = 11 obtained by curve fitting.

3.3.3. Tests with constant deviatoric stress

The GSD for the test at constant deviatoric stress CYC-CDS (**Series 3**) is shown in Fig. 9. In this test, the sample was sheared up to q = 180 kPa with ε_a = 0.1 % and p' = 460 kPa after an

isotropic compression up to 400 kPa; then it was stress-controlled by changing the axial stress and the confining stress simultaneously, keeping constant the value of q and varying p' from 460 kPa to 140 kPa (q/p' varies from 0.39 to 1.29, less than q/p'=1.46 of the constant-σ'_3 test at σ'_3=400 kPa) with three cycles. Such low values of q and p'_{max} were applied to ensure that little grain breakage would be caused by the applied stresses during the first loading. Therefore, the test can be used to investigate the influence of the stress ratio (changing between 0.39 and 1.29) on grain breakage. Note that the deviatoric stress varies from 190 to 170 kPa with an average value of 180 kPa due to the lack of very accurate test control; this average value is considered for the interpretation. The stress-strain curve in Fig. 9(a) and the volume change in Fig. 9(b) show that only small strains developed during the test. The increase of the volumetric strain during the stages of decreasing p' is mainly due to elastic unloading. The amount of grain breakage observed after testing was very small (Fig. 9c), which demonstrated that the cyclic change of stress ratios at moderate amplitudes had little influence on grain breakage.

3.4. Relation between grain breakage measures and plastic work

An energy input is needed for grains to break (see McDowell et al., 1996). We decided to adopt the plastic work as a measure of this energy and to link it to the breakage measures B_u and B_r^* representing the evolution of GSD. Under axisymmetric loading condition, the plastic work w_p defined in Eq. (2) can be expressed as follows

$$w_p = \int \left\langle p' \mathrm{d}\varepsilon_v^p + q \mathrm{d}\varepsilon_d^p \right\rangle \tag{7}$$

where $\mathrm{d}\varepsilon_v^p$ and $\mathrm{d}\varepsilon_d^p$ are the volumetric and deviatoric plastic strain increments, respectively. The plastic strain increment can be calculated by subtracting the elastic strain increment to the total strain increment ($\mathrm{d}\varepsilon^p = \mathrm{d}\varepsilon - \mathrm{d}\varepsilon^e$) with $\mathrm{d}\varepsilon_v^e = \mathrm{d}p'/K$ and $\mathrm{d}\varepsilon_d^e = \mathrm{d}q/(3G)$. Under axisymmetric condition, $\varepsilon_d = 2(\varepsilon_a - \varepsilon_r)/3$ and $q = (\sigma_a - \sigma_r)$. The Macaulay function in Eq. (7) implies that the negative plastic work due to shear induced dilation ($d\varepsilon_v^p < 0$) does not influence grain breakage.

Based on the stress-strain curves of all the above-mentioned tests, the plastic work was obtained by using Eqs. (3), (4) and (7). Then, B_u and B_r^* were plotted versus the plastic work, as shown in Fig. 10. For both monotonic and cyclic loading tests, the evolution of GSD can be

expressed by a unique function of the plastic work, independent of the loading condition

$$B_u = \frac{w_p}{a + w_p}; \quad B_r^* = \frac{w_p}{b + w_p} \tag{8}$$

with a = 6000 and b = 1000. Eq. (8) implies that the two breakage indexes increase asymptotically to the value of 1 when the plastic work increases. There is no further breakage once the ultimate grading is reached, which agrees with Coop et al. (2004).

Therefore, the plastic work appears to be a suitable variable to determine B_u and B_r^*, and therefore the evolution of the GSD, for different stress paths under both monotonic and cyclic loadings.

4. INFLUENCE OF GRAIN BREAKAGE ON THE EVOLUTION OF CSL

In the literature, three main methods for describing the influence of grain breakage on the CSL have been developed: (1) movement of CSL with the amount of plastic work (e.g., Biarez and Hicher, 1997; Daouadji et al., 2001); (2) direct description of CSL by one or several segments for different stress levels (e.g., Coop, 1990; Russell and Khalili, 2004; Bopp and Lade, 2005); (3) movement of CSL with the change of the grading state index I_G (see Kikumoto et al., 2010). The concept of the CSL is based on the assumption that at the critical state the material remains at a constant volume while being subjected to continuous distortion. If ever the CSL is able to move with the change of grading due to grain breakage during loading, this concept becomes dynamic and its evolution needs to be specified. This study specifies the concept of critical state along above studies by defining the position of the CSL at a given loading stage, corresponding to the present gradation.

For the tested material, in order to investigate whether the CSL moves or not when grain breakage occurs, drained triaxial tests at a confining stress of 100 kPa but with different stress histories (Fig. 11a) and tests with constant σ'_3 and constant p' (Fig. 11c) were carried out (see Section 3.2.3). Based on the e-logp' curves of the two tests in Fig. 11(a) with different amount of grain breakage (Fig. 6c), the hypothesis of a shift of the CSL can be justified. If we assume that the CSL evolves with grain breakage, we need to determine its initial position. For the limestone

grain material, it is difficult to measure the initial location of CSL, because it is very easily crushed even during triaxial tests at low confinement. We assumed that the test performed at the very low confining stress of 22 kPa could indicate the location of the initial CSL because the amount of crushing, if not completely null, was very limited and could not provoke a significant change in the GSD (Fig. 6c).

Furthermore, it is debatable on whether the slope of CSL is dependent or not on the GSD (Biarez and Hicher, 1997; Daouadji et al., 2001; Bandini and Coop, 2011). For the sake of simplicity, we assumed in this study a constant slope of CSL. This trend is also in agreement with the change of the CSL with gradation found when fines are added to sands for a limited stress level (Thevanayagam et al., 2002). Therefore, the CSL ca, be written:

$$e_c = e_{ref} - \lambda_c \ln\left(\frac{p'}{p_{at}}\right) \tag{9}$$

where e_c is the critical void ratio corresponding to the current p'; e_{ref} is the reference critical void ratio for a reference stress (taken equal to p_{at} for convenience); λ_c is the slope of the critical state line in the e-lnp' plane (Fig. 11b).

Test results under different confining stresses in Fig. 11(b) show the shift of CSL with increasing confining stress due to increasing amount of grain breakage (Fig. 4c). Fig. 11(c) shows that the CSL for the constant σ'_3 test (σ'_3 = 400 kPa) is lower than that for the constant p' test (p' = 400 kPa) due to more amount of grain breakage in the former test (Fig. 5c). Note that for the tests under high confining stresses it is difficult to reach the critical state (Fig. 4). In fact, as indicated by Bandini and Coop (2011) for crushable granular materials, a second (i.e. unloading and shearing) loading phase is usually needed to measure the critical state line. However, the tested limestone grains are easily crushed even under low confining pressures (Fig.4c). Therefore, in this study the final states at strain level of 25% for all tests were used to represent the “dynamic” critical state. This specific treatment does not affect the trend of the shift in the CSL. If the reference critical void ratio for each test is plotted as a function of the breakage measures B_u and B_r^* (Fig. 12b), the evolution of the CSL location can be linked to the evolution of GSD, as follows:

$$e_{ref} = e_{ref\,0} - \Delta e_{ref} \frac{B_u}{c + B_u} \quad ; \quad e_{ref} = e_{ref\,0} - \Delta e_{ref} \frac{B_r^*}{d + B_r^*} \tag{10}$$

with e_{ref0} = 1.43, Δe_{ref} = 0.5, c = 0.006 and d = 0.035 obtained by curve fitting. The proposed formulation for the evolution of the CSL location with the grain breakage measures takes a different form than the one proposed by Kikumoto et al. (2010) with the grading state index I_G.

Substituting Eq. (8) into Eq. **Error! Reference source not found.**, the reference critical void ratio can also be directly related to the plastic work, as follows

$$e_{ref} = e_{ref\,0} - \Delta e_{ref} \frac{w_p}{ac + (1+c) w_p} \quad ; \quad e_{ref} = e_{ref\,0} - \Delta e_{ref} \frac{w_p}{bd + (1+d) w_p} \tag{11}$$

In Eq. **Error! Reference source not found.**, the values of (1+c) and (1+d) can be taken approximately equal to 1 because the values of c and d are much smaller than 1. Thus, only ac and bd control the evolution rate of the CSL location with the plastic work. It was found that the fitting curves based on B_u and B_r^* in Fig. 12(c) are very close with ac = 39 (based on Figs. 10a, 12a) and bd = 35 (based on Figs. 10b, 12b). It should be noted that the CSL location cannot be directly measured in cyclic tests. If we assume that the results obtained from monotonic tests hold for more general loading condition, then the CSL location for cyclic tests can be estimated by using Fig. 12(c) and Eq. **Error! Reference source not found.**. This is a reasonable assumption, since the grain breakage measures appear to be a unique function of the plastic work for various loading conditions including monotonic and cyclic loadings (Eq. 8).

Therefore, it appears suitable to use the breakage measures B_u and B_r^* to determine the CSL location, which is of practical importance for constitutive modelling.

5. APPLICATION OF RELATIONS TO OTHER GRANULAR MATERIALS

The above relations between breakage measures, plastic work and CSL location based on the results obtained on the limestone grain material were applied to other materials: granite fragments (Kim, 1995), Cambria sand (Bopp and Lade, 2005; Lade and Bopp, 2005; Yamamuro and Lade, 1996), and Sydney sand (Russell and Khalili, 2004).

5.1. VALIDATION FOR DIFFERENT CRUSHABLE MATERIALS

The granite fragments consist of sub-angular grains (made of quartz with feldspars) with sizes between 0.3 mm and 2 mm. The material has an initial uniformity coefficient C_u = 2.0, a median grain size D_{50} = 0.85 mm and a specific gravity G_s = 2.65 g/cm^3. The minimum and maximum void ratios are 0.83 and 1.23, respectively. The initial e_{ref0} = 1.28 and λ_c = 0.088 were obtained adopting the correlation by Biarez and Hicher (1997). The relative uniformity, modified relative breakage index, CSL location and applied plastic work were obtained using drained triaxial tests carried out by Kim (1995) with confining stress of respectively 1 MPa, 5 MPa, 10 MPa, 30 MPa and 60 MPa.

Cambria sand consists of sub-rounded grains (made of quartz with small quantity of gypsum) with sizes between 0.83 mm and 2 mm, a median grain size D_{50} = 1.43 mm and with an initial uniformity coefficient C_u = 1.3. The minimum and maximum void ratios are 0.503 and 0.792, respectively. The specific gravity is G_s = 2.69 g/cm^3. The initial e_{ref0} = 0.73 and λ_c = 0.088 were measured from drained and undrained triaxial tests under low confining pressures (100, 200, 500 kPa) with no change of grading (Yamamuro and Lade, 1996), thus Biarez and Hicher's correlation is not needed. The relative uniformity, modified relative breakage index, CSL location and applied plastic work were obtained using drained and undrained triaxial tests under high confining pressures up to 52 MPa (Bopp and Lade, 2005; Lade and Bopp, 2005; Yamamuro and Lade, 1996).

Sydney sand is a predominantly quartz sand collected from sand dunes at Kurnell, Sydney. The sand has a median grain size D_{50} = 0.31 mm, initial uniformity coefficient C_u = 1.83, specific gravity G_s = 2.65 g/cm^3. The minimum and maximum void ratios are 0.60 and 0.92, respectively. The initial e_{ref0} = 0.97 and λ_c = 0.07 were obtained from drained and undrained triaxial tests under low confining pressures (50, 150 and 200 kPa) with no change of grading (Russell and Khalili, 2004). The relative uniformity, modified relative breakage index, CSL location and applied plastic work were obtained using drained and undrained triaxial tests under high confining pressures up to 7.8 MPa (Russell and Khalili, 2004).

Using Eq. (8), the relative uniformity and the modified relative breakage index were plotted versus the applied plastic work in Figs. 13(a) and 13(b) respectively, for the three granular materials. Furthermore, using Eq. **Error! Reference source not found.**, the reference critical void ratio was plotted with the relative uniformity and the modified relative breakage index in Figs. 13(c) and 13(d), respectively. Comparisons between experimental results and calculations demonstrate that the proposed relationships based on limestone grains are also suitable for other crushable granular materials.

5.2. Analysis of mineral component effect on grain breakage

As shown in Fig. 13, the values of a, b, c and d control the breakage amount and the CSL location, and thus can represent the ease of grain breakage and its effect on the mechanical behaviour of granular materials. The ease of grain breakage depends on several parameters linked to grain nature, grain size distribution, assembly void ratio. It has been shown by different authors that a badly graded material is more prone to grain breakage than a well graded one (see Lee and Farhoomand, 1967; Biarez and Hicher, 1997; Muir Wood and Maeda, 2007). For a given material more grain breakage occurs for a same stress amplitude when the void ratio is larger. This last result can be connected to the fact that a lower coordination number creates a higher concentration of the inner forces applied to the grains. There are several parameters describing the grain nature (Lo and Roy, 1973; Hardin, 1985; Coop, 1990; Lade et al., 1996; Nakata et al., 1999; Leleu and Valdes, 2007): mineralogy, shape, size, degree of alteration, and so on. All these parameters play a significant role in the crushing of the grains. In this study we focus on the influence of the mineralogy, which is an important factor relating to the grain breakage according to Lo and Roy (1973) and Leleu and Valdes (2007). The granular materials examined above have all similar grain sizes and similar grain size distributions characterized by a uniformity coefficient C_u between 1.3 and 2. We will, therefore, examine the eventual links between the values of the material constants determined previously and the grain mineral components. In order to examine the possible links, we carried out analyses of the mineral components of the selected materials.

449 The Mohs scale characterizes mineral hardness, and it is often adopted to represent the
450 nature of the mineral constituting the rock material. Because of a lack of data concerning the
451 individual grain strength for the selected sands, we adopted in this study the Mohs hardness as a
452 mineral index to investigate the mineral effect on the rate of grain breakage due to plastic work
453 and the rate of CSL movement due to grain breakage. It is clear that this index can only be
454 considered as a rough estimate of the mechanical properties of the grains. According to their
455 mineral contents, the values of hardness for all selected materials were estimated based on
456 Cordua's work (Cordua, 1998) as follows: (1) For the limestone grains, the hardness is estimated
457 between 3 and 4 with an average value of 3.5; (2) for the granite fragments consisting of quartz
458 with feldspars, the hardness of quartz is 7 and the hardness of feldspars varies from 2 to 6
459 depending on weathering. Thus, we retained a hardness varying from 4.5 to 6.5 with an average
460 value of 5.5; (3) for Cambria sand consisting of quartz with a small quantity of gypsum, the
461 hardness of gypsum is 2. Assuming that less than 10 % of gypsum exists in Cambria sand, we
462 retained a hardness varying from 6.5 to 7 with an average value of 6.75; (4) for Sydney sand
463 which is predominantly a quartz sand, we retained a hardness of 7.

464 The values for the constants *a*, *b*, *c* and *d* were plotted versus Mohs' hardness ranges and
465 mean values for all selected materials in Fig. 14. The evolutions of *a*, *b*, *c* and *d* with the
466 hardness appear all similar (Figs. 14a-b). The values of *ac* and *bd* are very close for each material,
467 as already obtained for limestone grains (Fig. 14c). The evolution of *ac* and *bd* with the hardness
468 follows the same pattern as the ones obtained for each individual constant and can be expressed
469 by the following equation

470 $$y = \beta e^{\omega H_m} \tag{12}$$

471 where y represents a, b, c, d, ac or bd; H_m is Mohs' harness; the values of the parameters β and ω
472 can be determined from Fig. 14. For instance, for *ac* or *bd* we obtained: β = 0.33 and
473 $\omega = 1.33$. From Fig. 14, we can conclude that the mineral component may also be a very
474 important factor influencing the grain breakage of materials.

6. CONCLUSIONS

Clasts fragmentation is a key issue in assessing the evolution of mechanical properties of granular materials subjected to compression and shearing, especially under high confining stresses and dynamic loadings, such as those that can occur during the runout of rock and debris avalanches. In this work, we first discussed existing measures for the amount of grain breakage. We selected the modified relative breakage index B_r^* by Einav (2007) as a convenient measure for the engineering practice. For more convenience, we proposed the use of the relative uniformity B_u, based on the evolution of the uniformity coefficient C_u, that is widely used to characterize the GSD.

Triaxial tests with different stress paths under both monotonic and cyclic loadings on limestone grain assemblies have been carried out. Based on experimental observations, the evolution of the breakage measures B_u and B_r^* have been shown to be both a hyperbolic function of the plastic work, independently of the nature of the loading. Furthermore, the shift of the critical state line due to grain breakage was also investigated. Based on the results obtained on the limestone grains, a relation between the breakage measures and the CSL location was proposed. In this way, the shift of the CSL can be determined at any stage of a mechanical loading by calculating the plastic work.

The relations between breakage measures, plastic work and CSL location were applied to other granular materials: granite fragments, Cambria sand and Sydney sand. The results showed that the relations based on limestone grains were also suitable for other crushable granular materials.

ACKNOWLEDGEMENTS

This research was supported by the National Basic Research Program of China: the funds for creative research groups of China (41521002) and the basic research funds (41790433). The work was also supported by the Sichuan funding for young researchers (2016JQ0021).

REFERENCES

Bandini, V., Coop, M. R., 2011. The influence of particle breakage on the location of the critical state line of

sands. Soils and Foundations, 51(4):591-600, doi: 10.3208/sandf.51.591.

Been, K., Jefferies, M. G., 1985. A state parameter for sands. Géotechnique 35(2): 99-112.

Biarez, J., Hicher, P.-Y., 1997. Influence de la granulométrie et de son évolution par ruptures de grains sur le comportement mécanique de matériaux granulaires. Revue Française de Génie Civil, 1(4):607-631.

Bolton, M. D., Nakata, Y., Cheng, Y. P., 2008. Micro- and macro-mechanical behaviour of DEM crushable materials. Géotechnique 58(6): 471-480.

Bopp, P. A., Lade, P. V., 2005. Relative density effects on undrained sand behavior at high pressures. Soils and Foundations 45(1): 15-26.

Bowman, E., Take, W. A., de Graaf, K., Hann, C., 2012. Physical models of rock avalanche spreading behaviour with dynamic fragmentation. Canadian Geotechnical Journal, 49(4):460-476, doi: 10.1139/t2012-007.

Cecconi, M., De Simone, A., Tamagnini, C., Viggiani, G. M. B., 2002. A constitutive model for granular materials with grain crushing and its application to a pyroclastic soil. International Journal for Numerical and Analytical Methods in Geomechanics, 26(15):1531-1560, doi: 10.1002/nag.257.

Cheng, Y. P., Nakata, Y., Bolton, M. D., 2003. Discrete element simulation of crushable soil. Géotechnique 53(7):633-641, doi: 10.1680/geot.2003.53.7.633.

Clayton, C. R. I., 2010. Stiffness at small strain: research and practice. Géotechnique 61(1): 5-37.

Coop, M. R., 1990. The mechanics of uncemented carbonate sands. Géotechnique 40(4): 607–626.

Coop, M. R., Altuhafi, F., 2011. Changes to particle characteristics associated with the compression of sands. Géotechnique, 61(6):459-471, doi: 10.1680/geot.9.P.114.

Coop, M. R., Sorensen, K. K., Bodas Freitas, T., Georgoutsos, G., 2004. Particle breakage during shearing of a carbonate sand. Géotechnique, 54(3):157-163, doi: 10.1680/geot.2004.54.3.157.

Cordua, W. S., 1998. The Hardness of Minerals and Rocks. Lapidary Digest. Hosted at International Lapidary Association.

Crosta, G. B., Frattini, P., Fusi, N., 2007. Fragmentation in the Val Pola rock avalanche, Italian Alps. Journal of Geophysical Research: Atmospheres, 112(F1), doi: 10.1029/2005JF000455.

Dai, K., Li, Z., Tomas, R., et al., 2016. Monitoring activity at the Daguangbao mega-landslide (China) using Sentinel-1 TOPS time series interferometry. Remote Sensing of Environment 186:501-513, doi: 10.1016/j.rse.2016.09.009.

Daouadji, A., Hicher, P.-Y., Rahma, A., 2001. An elastoplastic model for granular materials taking into account grain breakage. European Journal of Mechanics-A/Solids, 20(1):113-137, doi: 10.1016/S0997-7538(00)01130-X.

Davies, T. R., McSaveney, M. J., 2002. Dynamic simulation of the motion of fragmenting rock avalanches. Canadian Geotechnical Journal, 39:789-798, doi: 10.1139/t02-035.

Davies, T. R., McSaveney, M. J., 2016. Comment on “The Reduction of Friction in Long-Runout Landslides as an Emergent Phenomenon” by Brandon C. Johnson, Charles S. Campbell, and H. Jay Melosh. Journal of Geophysical Research: Earth Surface, doi: 10.1002/2016JF003954.

Davies, T. R., McSaveney, M. J., Hodgson, K. A., 1999. A fragmentation-spreading model for long-runout rock avalanches. Canadian Geotechnical Journal, 36:1096-1110, doi: 10.1139/t99-067.

De Blasio, F. V., Crosta, G. B., 2015. Fragmentation and boosting of rock falls and rock avalanches. Geophysical Research Letters, doi: 10.1002/2015GL064723.

Deganutti, A. M., 2008. The hypermobility of rock avalanches. PhD Thesis, supervisor: prof. R. Genevois, University of Padova, Italy, http://paduaresearch.cab.unipd.it/682/

545 Dufresne, A., Dunning, S., 2017. Process dependence of grain size distributions in rock avalanche deposits.
546 Landslides, doi: 10.1007/s10346-017-0806-y.

547 Einav, I., 2007. Breakage mechanics- Part I: Theory. Journal of the Mechanics and Physics of Solids,
548 55(6):1274-1297, doi: 10.1016/j.jmps.2006.11.003.

549 Evans, S. G., Guthrie, R. H., Roberts, N. J., Bishop, N. F., 2007. The disastrous 17 February 2006
550 rockslide-debris avalanche on Leyte Island, Philippines: a catastrophic landslide in tropical mountain
551 terrain, Nat. Hazards Earth Syst. Sci., 7, 89—101, doi: 10.5194/nhess-7-89-2007.

552 Fan, X., Xu, Q., Scaringi, G., et al., 2017. Failure mechanism and kinematics of the deadly June 24th 2017
553 Xinmo landslide, Maoxian, Sichuan, China. Landslides 14(6):2129-2146, doi:
554 10.1007/s10346-017-0907-7.

555 Gorum, T., Fan, X., Van Westen, C. J., et al., 2011. Distribution pattern of earthquake-induced landslides
556 triggered by the 12 May 2008 Wenchuan earthquake. Geomorphology 133:152-167, doi:
557 10.1016/j.geomorph.2010.12.030.

558 Hardin, B. O., 1985. Crushing of soil particles. Journal of Geotechnical Engineering ASCE,
559 111(10):1177-1192.

560 Harireche, O., McDowell, G. R., 2003. Discrete element modelling of cyclic loading of crushable aggregates.
561 Granular Matter 5(3):147-151, doi: 10.1007/s10035-003-0143-9.

562 Head, K. H., 1992. Manual of soil laboratory testing, Volume 3: Effective stress tests, second edition. John
563 Wiley & Sons, New York, pp 428.

564 Hicher, P.-Y., 1996. Elastic properties of soils. Journal of Geotechnical Engineering ASCE 122(8): 641-648.

565 Hu, W., Hicher, P.-Y., Scaringi, G., et al., 2017a. Seismic precursor to instability induced by internal erosion in
566 loose granular slopes. Géotechnique, doi: 10.1680/jgeot.17.p.079.

567 Hu, W., Huang, R., McSaveney, M., et al., 2018. Mineral changes quantify frictional heating during a large
568 low-friction landslide. Geology, doi: 10.1130/G39662.1.

569 Hu, W., Scaringi, G., Xu, Q., et al., 2017b. Sensitivity of the initiation and runout of flowslides in loose
570 granular deposits to the content of small particles: An insight from flume tests. Engineering Geology
571 231:34-44, doi: 10.1016/j.enggeo.2017.10.001.

572 Hu, W., Xu, Q., Wang, G., et al., 2015. Sensitivity of the initiation of debris flow to initial soil moisture.
573 Landslides 12(6):1139-1145, doi: 10.1007/s10346-014-0529-2.

574 Huang, R., Fan, X., 2013. The landslide story. Nature Geoscience 6:325–326, doi: 10.1038/ngeo1806.

575 Huang, R., Pei, X., Fan, X., et al., 2012. The characteristics and failure mechanism o the largest landslide
576 triggered by the Wenchuan earthquake, May 12, 2008, China. Landslides 9:131-142, doi:
577 10.1007/s10346-011-0276-6.

578 Hungr, O., Leroueil, S., Picarelli, L., 2014. The Varnes classification of landslide types, an update. Landslides
579 11(2):167-194, doi: 10.1007/s10346-013-0436-y.

580 Imre, B., Laue, J., Springman, S. M., 2010. Fractal fragmentation of rocks within sturzstroms: insight derived
581 from physical experiments within the ETH geotechnical drum centrifuge. Granular Matter, 12:267-285,
582 doi: 10.1007/s10035-009-0163-1.

583 Indraratna, B., Vinod, J. S., Lackenby, J., 2009. Influence of particle breakage on the resilient modulus of
584 railway ballast. Géotechnique, 59(7):643-646, doi: 10.1680/geot.2008.T.005.

585 Jiang, Y., Wang, G., Kamai, T., 2016. Fast shear behavior of granular materials in ring-shear tests and
586 implications for rapid landslides. Acta Geotechnica, doi: 10.1007/s11440-016-0508-y.

587 Johnson, B. C., Campbell, C. S., Melosh, H. J., 2015. The reduction of friction in long runout landslides as an
588 emergent phenomenon. Journal of Geophysical Research: Earth Surface, doi: 10.1002/2015JF003751.

589 Jovicic, V., Coop, M. R., 1997. Stiffness of coarse-grained soils at small strains. Géotechnique 47(3): 545-561

590 Kaproth, B. M., Cashman, S., Marone, C., 2010. Deformation band formation and strength evolution of
591 unlithified sand: The role of grain breakage. Journal of Geophysical Research: Atmospheres, 115(B12),
592 doi: 10.1029/2010JB007406.

593 Keefer, D. K., Larsen, M. C., 2007. Assessing landslide hazards. Science 316:1136-1138, doi:
594 10.1126/science.1143308.

595 Kikumoto, M., Muir Wood, D., Russell, A. R., 2010. Particle crushing and deformation behaviour. Soils and
596 Foundations, 50(4):547-563, doi: 10.3208/sandf.50.547.

597 Kim, M. S., 1995. Etude expérimentale du comportement mécanique des matériaux granulaires sous fortes
598 contraintes. Thèse de Doctorat, École Centrale de Paris.

599 Kimura, S., Kaneko, H., Ito, T., Minagawa, H., 2014. The Effect of Effective Normal Stress on Particle
600 Breakage, Porosity and Permeability of Sand: Evaluation of Faults around Methane Hydrate Reservoirs.
601 Tectonopysics 630(1), doi: 10.1016/j.tecto.2014.05.031.

602 Koi, T., Hotta, N., Ishigaki, I., et al., 2008. Prolonged impact of earthquake-induced landslides on sediment
603 yield in a mountain watershed: The Tanzawa region, Japan. Geomorphology 101:692-702, doi:
604 10.1016/j.geomorph.2008.03.007.

605 Lade, P. V., Bopp, P. A., 2005. Relative density effects on drained sand behaviour at high pressures. Soils and
606 Foundations 45(1): 1-13.

607 Lade, P. V., Yamamuro, J. A., Bopp, P. A., 1996. Significance of particle crushing in granular materials. Journal
608 of Geotechnical Engineering ASCE 122(4):309-316.

609 Lee, K. L., Farhoomand, I., 1967. Compressibility and crushing of granular soil in anisotropic triaxial
610 compression. Canadian Geotechnical Journal, 4(1):68-86, doi: 10.1139/t67-012.

611 Leleu, S. L., Valdes, J. R., 2007. Experimental study of the influence of mineral composition on sand crushing.
612 Géotechnique 57(3): 313-317.

613 Liu, S., Wang, Y., Shen, C., 2017. DEM analysis of granular crushing during simple shearing. Marine
614 Georesources and Geotechnology, doi: 10.1080/1064119X.2017.1349846.

615 Lo, K. Y., Roy, M., 1973. Response of particulate materials at high pressures. Soils and Foundations 13(1):
616 61-76.

617 Locat, P., Couture, R., Leroueil, S., Locat, J., Jaboyedoff, M., 2006. Fragmentation energy in rock avalanches.
618 Canadian Geotechnical Journal, 43(8):830-851, doi: 10.1139/T06-045.

619 Lucas, A., Mangeney, A., Ampuero, J. P., 2014. Frictional velocity-weakening in landslides on Earth and on
620 other planetary bodies. Nature Communications, 5(3417), doi: 10.1038/ncomms 4417.

621 Ma, G., Zhou, W., Regueiro, R. A., Wang, Q., Chang, X., 2017. Modeling the fragmentation of rock grains
622 using computed tomography and combined FDEM. Powder Technology, 308:388-397, doi:
623 10.1016/j.powtec.2016.11.046.

624 Marsal, R. J., 1967. Large-scale testing of rockfills materials. Journal of the Soil Mechanics and Foundation
625 Engineering ASCE, 93(2):27-44, doi:

626 McDowell, G. R., Bolton, M. D., 1998. On the micromechanics of crushable aggregates. Géotechnique,
627 48(5):667-679, doi: 10.1680/geot.1998.48.5.667.

628 McDowell, G. R., Lu, M., 2010. Discrete element modelling of railway ballast under monotonic and cyclic
629 triaxial loading. Géotechnique, 60(6):459-467, doi: 10.1680/geot.2010.60.6.459.

630 McDowell G. R., M. D. Bolton, and D. Robertson (1996). Fractal crushing of granular materials. Journal of the
631 mechanics and physics of solids, 44(12):2079-2102.

McSaveney, M. J., 2015. Fragmenting Granular Flow: A Personal Account of the Concept. In: Lollino G. et al. (eds) Engineering Geology for Society and Territory - Volume 2. Springer, Cham, doi: 10.1007/978-3-319-09057-3_308.

McSaveney, M. J., Davies, T. R., 2006. Rapid rock mass flow with dynamic fragmentation: Inferences from the morphology and internal structure of rockslides and rock avalanches. In: Evans S.G., Mugnozza G.S., Strom A., Hermanns R.L. (eds) Landslides from -Massive Rock Slope Failure. NATO Science Series, vol 49. Springer, Dordrecht, doi: 10.1007/978-1-4020-4037-5_16.

Miao, G., Airey, D. W., 2013. Breakage and ultimate states for a carbonate sand. Géotechnique 63(14):1221-1229, doi: 10.1680/geot.12.P.111.

Miura, N., Murata, H., Yasufuku, N., 1984. Stress–strain characteristics of sand in a particle crushing region. Soils and Foundations 24(1):77–89.

Muir Wood, D., Maeda, K., 2007. Changing grading of soil: effect on critical states. Acta Geotechnica 3: 3–14

Nadim, F., Kjekstad, O., Peduzzi, P., Herold, C., Jaedicke, C., 2006. Global landslide and avalanche hotspots. Landslides 3:159–173, doi: 10.1007/s10346-006-0036-1.

Nakata, Y., Hyde, A. F. L., Hyodo, M., Murata, H., 1999. A probabilistic approach to sand particle crushing in the triaxial test. Géotechnique, 49(5):567-583, doi: 10.1680/geot.1999.49.5.567.

Petley, D., 2012. Global patterns of loss of life from landslides. Geology 40(10):927-930, doi: 10.1130/G33217.1.

Richart, F. E., Hall, J. R., Woods, R. D., 1970. Vibration of Soils and Foundations. International Series in Theoretical and Applied Mechanics. Prentice-Hall: Englewood Cliffs, NJ.

Robinson, T. R., Davies, T. R., Reznichenko, N. V., De Pascale, G. P., 2015. The extremely long-runout Komansu rock avalanche in the Trans Alai range, Pamir Mountains, southern Kyrgyzstan. Landslides, 12(3):523-535, doi: 10.1007/s10346-014-0492-y.

Russell, A. R., Khalili, N., 2004. A bounding surface plasticity model for sands exhibiting particle crushing. Canadian Geotechnical Journal, 41(6):1179-1192, doi: 10.1139/t04-065.

Scaringi, G., Hu, W., Xu, Q., Huang, R., 2017. Shear-Rate-Dependent Behavior of Clayey Bimaterial Interfaces at Landslide Stress Levels. Geophysical Research Letters, doi: 10.1002/2017GL076214

Simonini, P., 1996. Analysis of Behavior of Sand Surrounding Pile Tips. Journal of Geotechnical Engineering ASCE, 122(11):897-905, doi: 10.1061/(ASCE)0733-9410(1996)122:11(897).

Taboada, A., Estrada, N., 2009. Rock-and-soil avalanches: Theory and simulation (2009). Journal of Geophysical Research, 114:F03004, doi: 10.1029/2008JF001072.

Tang, C., Van Asch, T. W. J., Chang, M., et al., 2012. Catastrophic debris flows on 13 August 2010 in the Qingping area, southwestern China: The combined effects of a strong earthquake and subsequent rainstorms. Geomorphology, 139–140:559–576, doi: 10.1016/j.geomorph.2011.12.021.

Thevanayagam, S., Shenthan, T., Mohan, S., Liang, J., 2002. Undrained Fragility of clean sands. Journal of Geotechnical and Geoenvironmental Engineering ASCE 128(10): 849-859.

Van Asch, T. W. J., Buma, J., Van Beek, P. H., 1999. A view on some hydrological triggering systems in landslides. Geomorphology 30:25–32, doi: 10.1016/S0169-555X(99)00042-2.

Wang, Y. F., Cheng, Q. G., Zhu, Q., 2015, Surface microscopic examination of quartz grains from rock avalanche basal facies. Canadian Geotechnical Journal, 52(2):167-181, doi: 10.1139/cgj-2013-0284.

Wang, Y. F., Dong, J. J., Cheng, Q. G., 2017. Velocity-dependent frictional weakening of large rock avalanche basal facies: Implications for rock avalanche hypermobility? Journal of Geophysical Research: Solid Earth, doi: 10.1002/2016JB013624.

Worth, C. P., Bassett, N. A., 1965. stress-strain relationship for the shearing behavior of sand. Géotechnique

15(1):32-56.

Xu, Q., Shang, Y. J., Van Asch, T. W. J., et al., 2012. Observations from the large, rapid Yigong rock slide-debris avalanche, southeast Tibet. Canadian Geotechnical Journal, 49(5): 589-606, doi: 10.1139/t2012-021.

Xu, Q., Zhang, S., Li, W. L., Van Asch, T. W. J., 2012. The 13 August 2010 catastrophic debris flows after the 2008 Wenchuan earthquake, China. Nat Hazards Earth Syst Sci 12:201–216, doi: 10.5194/nhess-12-201-2012.

Yamamuro, J. A., Lade, P. V., 1996. Drained sand behavior in axisymmetric tests at high pressures. Journal of Geotechnical Engineering ASCE 122(2): 109-119.

Yao, Y. P., Yamamoto, H., Wang, N. D., 2008. Constitutive model considering sand crushing. Soils and Foundations, 48(4):603-608, doi: 10.3208/sandf.48.603.

Zhang, M., McSaveney, M. J., 2017. Rock-avalanche deposits store quantitative evidence on internal shear during runout. Geophysical Research Letters, doi: 10.1002/2017GL073774.

Zhang, M., Yin, Y., McSaveney, M., 2016a. Dynamics of the 2008 earthquake-triggered Wenchuan Creek rock avalanche, Qingping, Sichuan, China, Engineering Geology 200:75-87, doi: 10.1016/j.enggeo.2015.12.008.

Zhang, S., Zhang, L., Lacasse, S., Nadim, F., 2016. Evolution of Mass Movements near Epicentre of Wenchuan Earthquake, the First Eight Years. Scientific Reports 6:36154, doi: 10.1038/srep36154.

Zhang, X., Baudet, B. A., 2013. Particle breakage in gap-graded soil. Géotechnique Letters, 3(2):72-77, doi: 10.1680/geolett.13.00022.

Zhang, X., Baudet, B. A., 2014. The multi-fractal nature of soil particle size distribution. In: Soga et al. (Eds.), Geomechanics from Micro to Macro, Taylor & Francis Group, London, pp. 1183-1188, doi: 10.1201/b17395-213.

Zhao, T., Crosta, G. B., Utili, S., De Blasio, F. V., 2017. Investigation of rock fragmentation during rockfalls and rock avalanches via 3-D discrete element analyses. J. Geophys. Res. Earth Surf., 122, doi:10.1002/2016JF004060.

Zhou, B., 2017. Discrete element modeling of crushable sands considering realistic particle shape effect. Computers and Geotechnics, 91:179-191, doi: 10.1016/j.compgeo.2017.07.016.

FIGURES

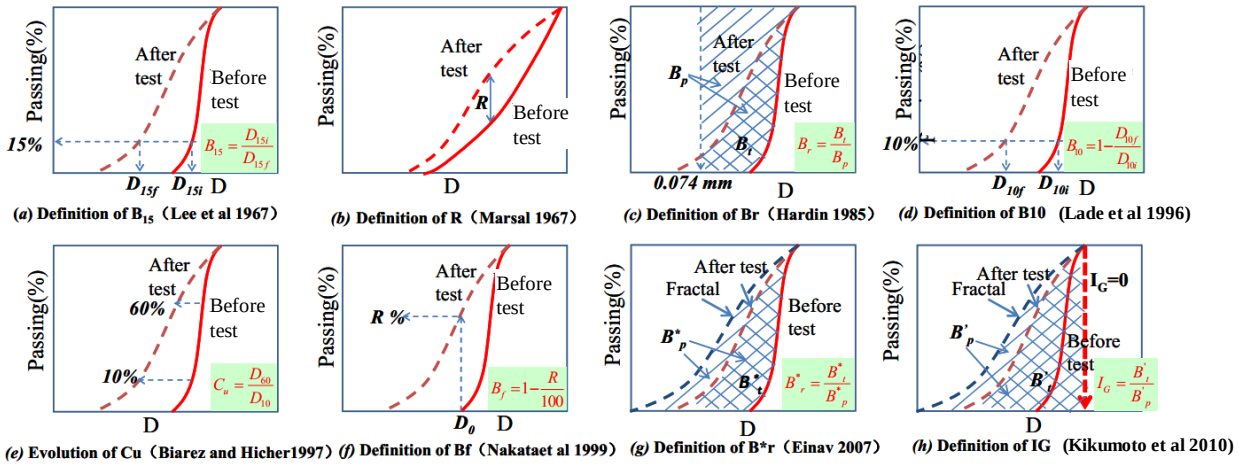

Fig. 1. Illustration of different measures of grain breakage.

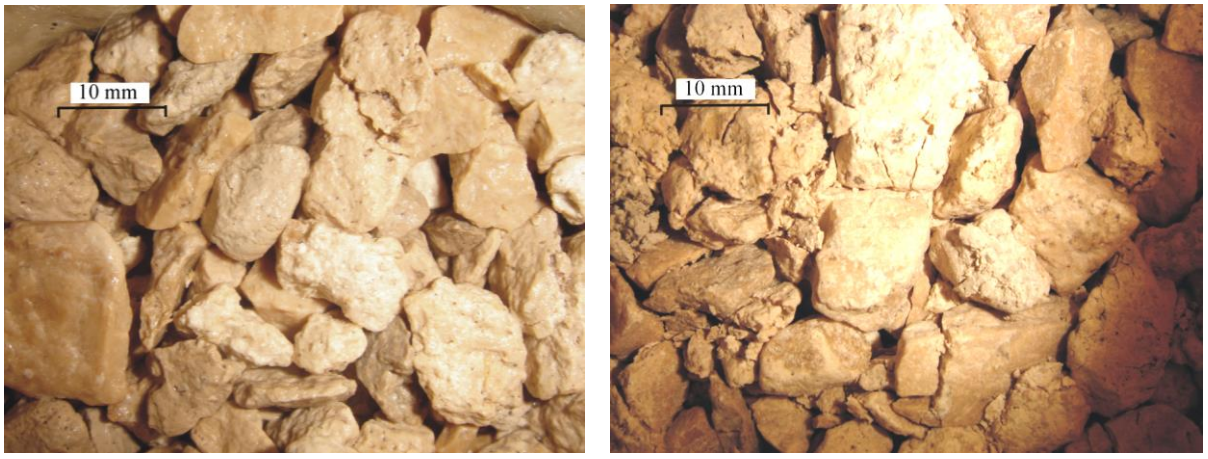

(a) **(b)**

Fig. 2. Photographs of a tested sample: (a) before testing, and (b) after testing under constant p' = 400 kPa.

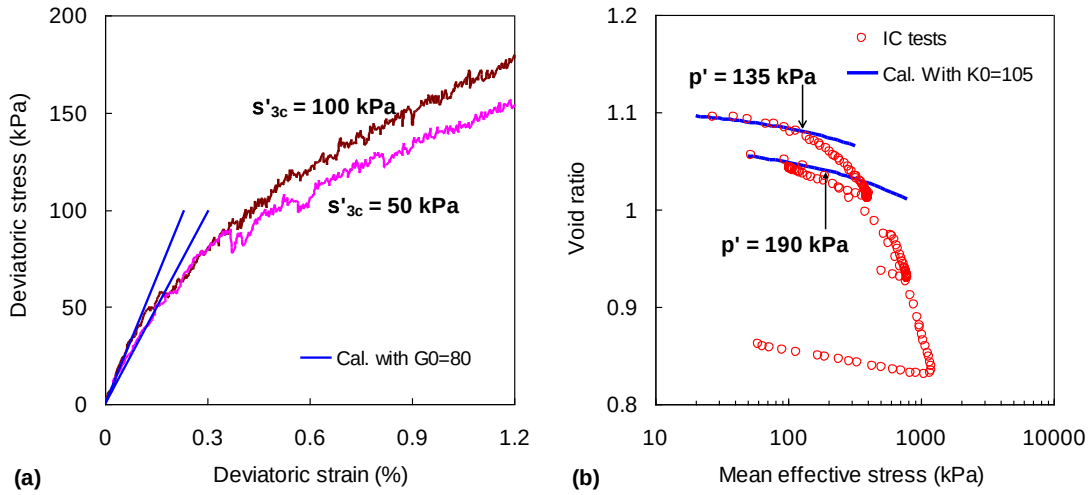

Fig. 3. (a) Deviatoric stress-strain curves of drained triaxial tests under constant confining stresses at 50 kPa and 100 kPa, and (b) isotropic compression tests in e-log(p') plane.

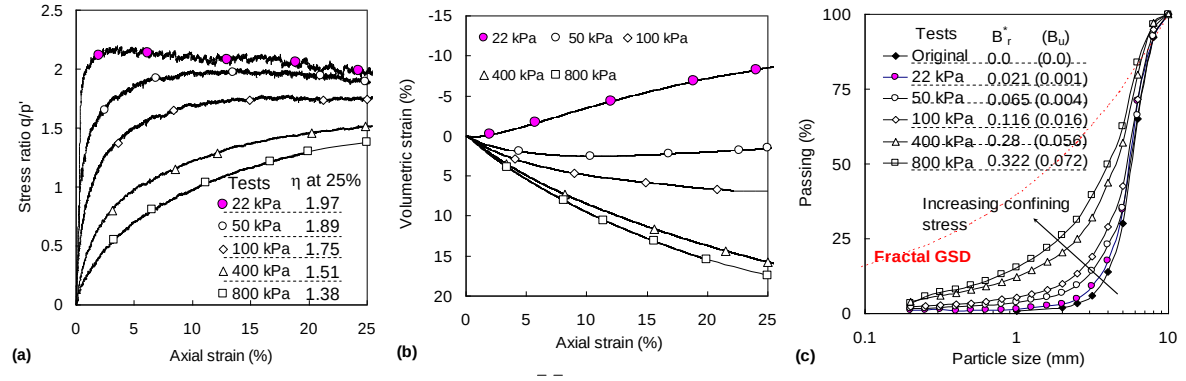

Fig. 4. Drained triaxial tests under constant confining stresses varying from 22 to 800 kPa: (a) stress ratio versus axial strain, (b) volumetric strain versus axial strain, (c) grain size distributions.

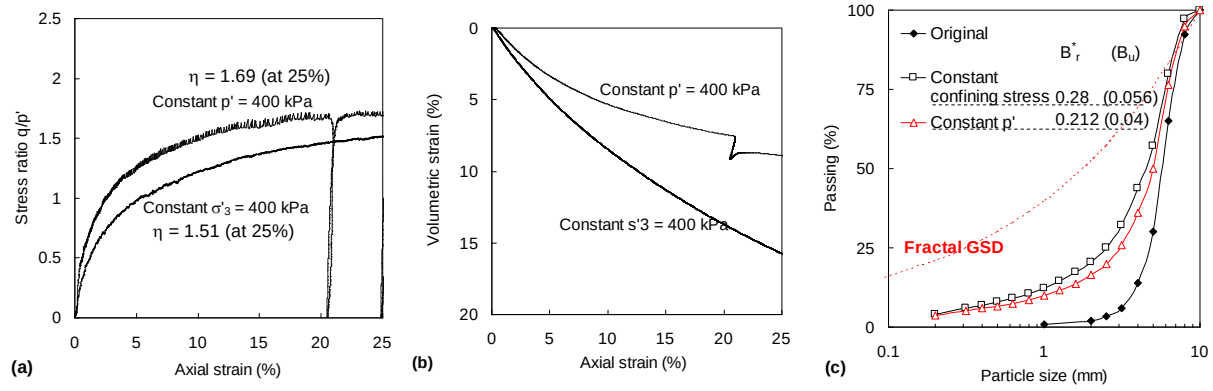

Fig. 5. Comparison of drained triaxial tests under constant confining stress and under constant p':

(a) stress ratio versus axial strain, (b) volumetric strain versus axial strain, (c) grain size distributions.

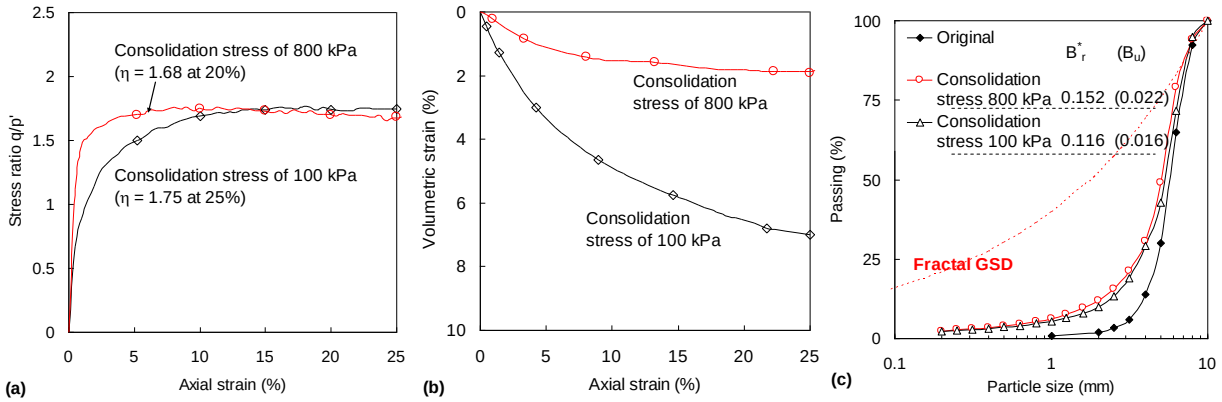

Fig. 6. Comparison of drained triaxial tests with different consolidation histories: (a) stress ratio versus axial strain, (b) volumetric strain versus axial strain, (c) grain size distributions.

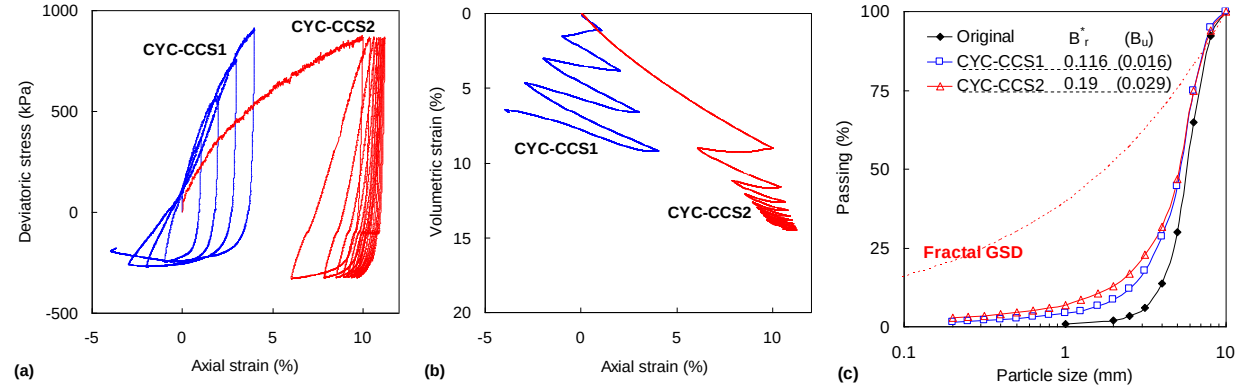

Fig. 7. Comparison of drained triaxial tests with different stress strain levels: (a) deviatoric stress versus axial strain, (b) volumetric strain versus axial strain, (c) grain size distributions.

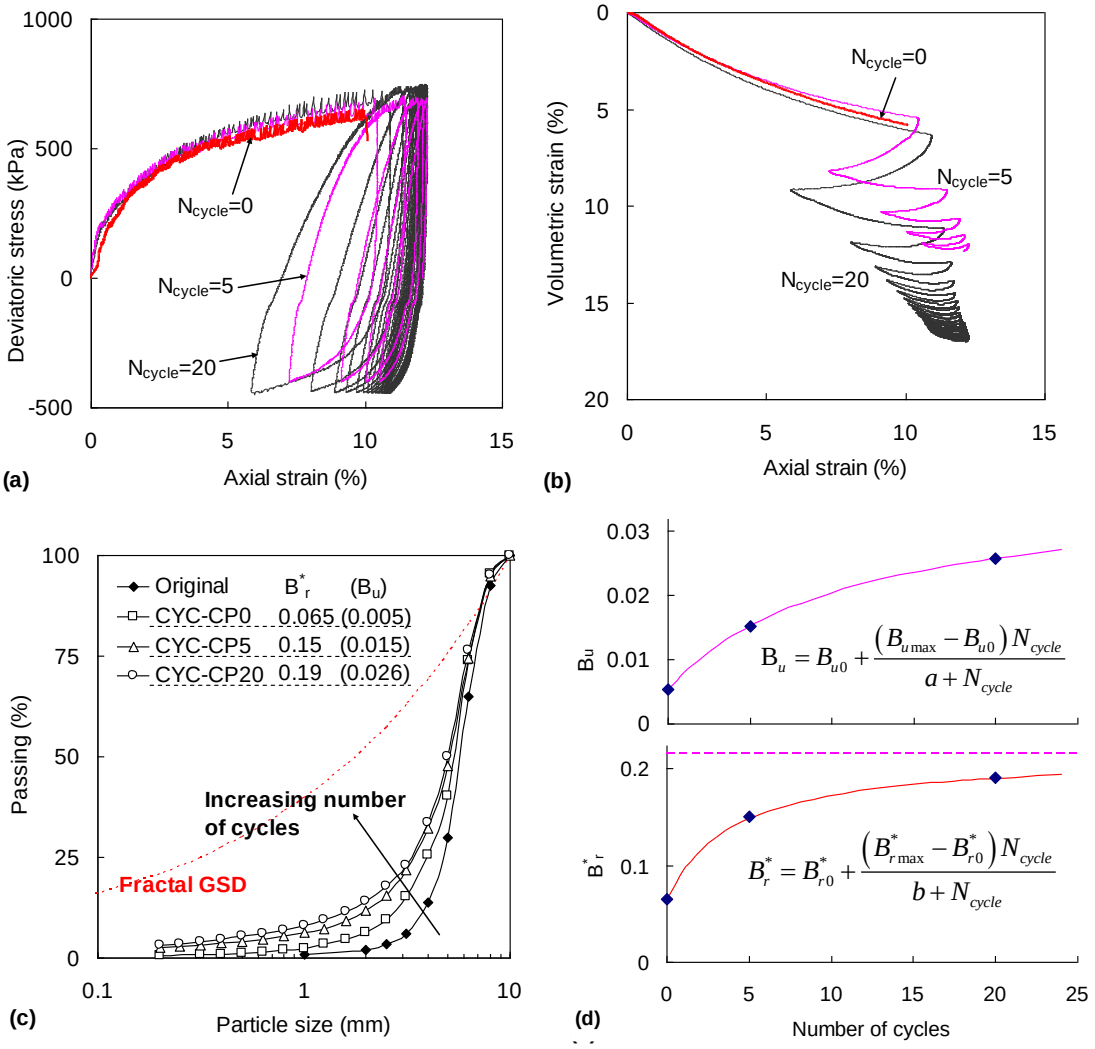

Fig. 8. Comparison of drained triaxial tests with different number of cycles: (a) deviatoric stress versus axial strain, (b) volumetric strain versus axial strain, (c) grain size distributions, (d) B_u and B^*_r versus number of cycles.

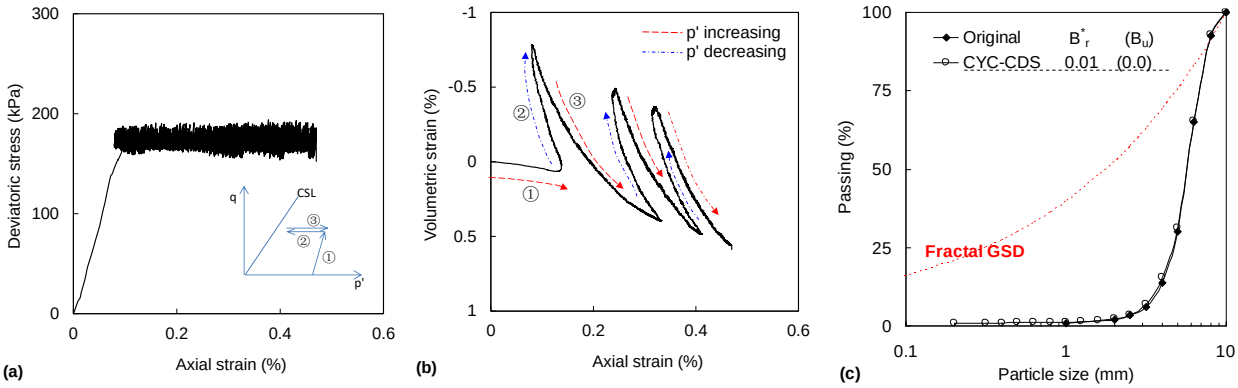

Fig. 9. Results of drained triaxial tests with constant deviatoric stress: (a) deviatoric stress versus

axial strain, (b) volumetric strain versus axial strain, (c) grain size distributions.

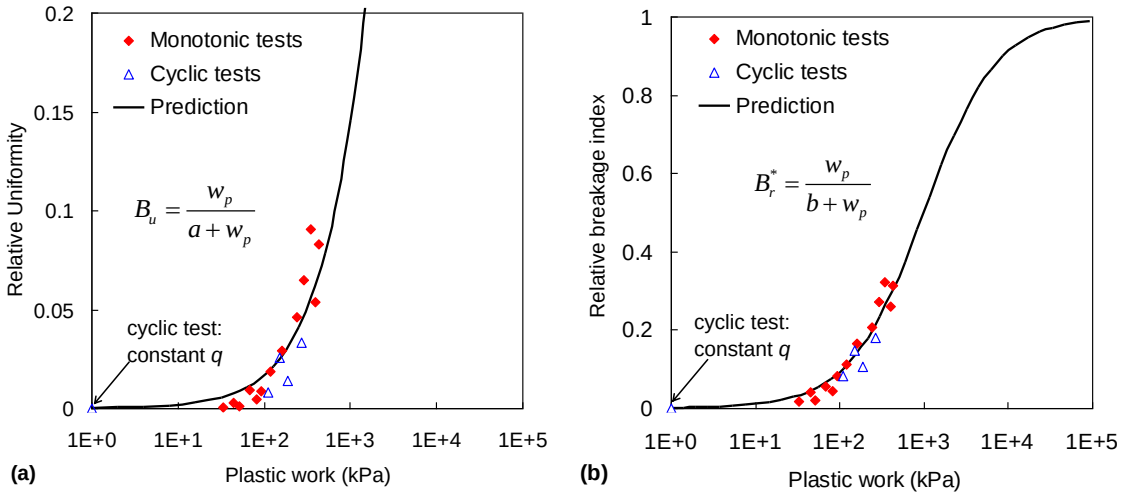

Fig. 10. (a) Relative uniformity versus plastic work, and (b) modified relative breakage index versus plastic work.

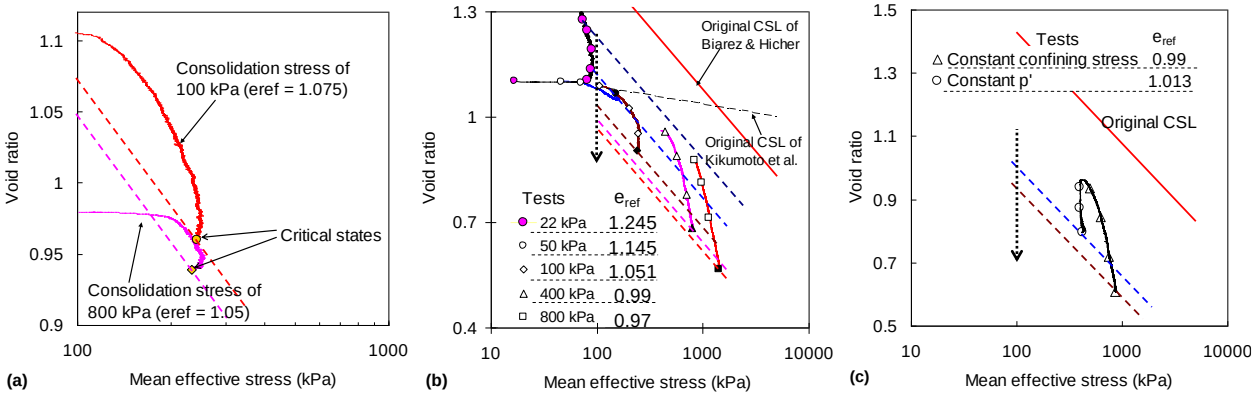

Fig. 11. Movement of CSL in e-log(p') plane for: (a) tests with different consolidation stress histories, (b) tests with different confining stresses, and (c) tests with different stress paths.

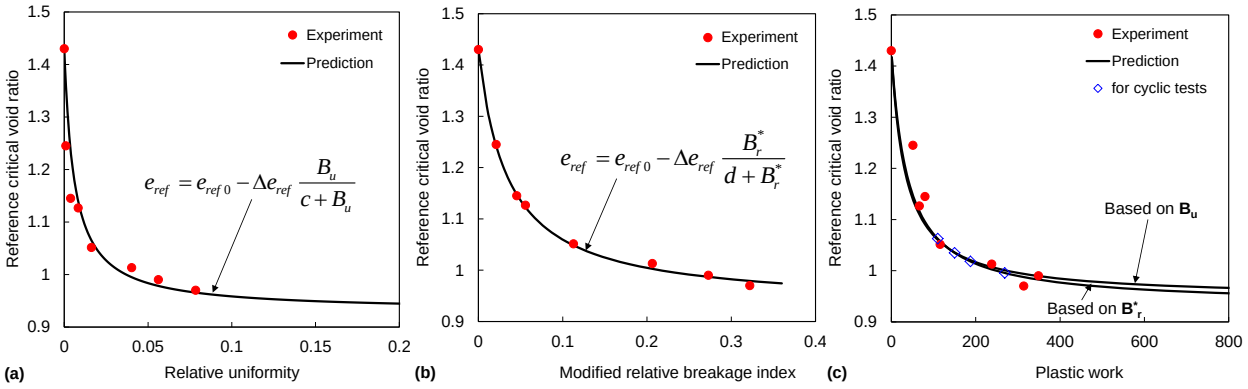

754
755 **Fig. 12.** (a) Reference critical void ratio versus relative uniformity, (b) Reference critical void
756 ratio versus modified relative breakage index, and (c) Reference critical void ratio versus plastic
757 work.
758

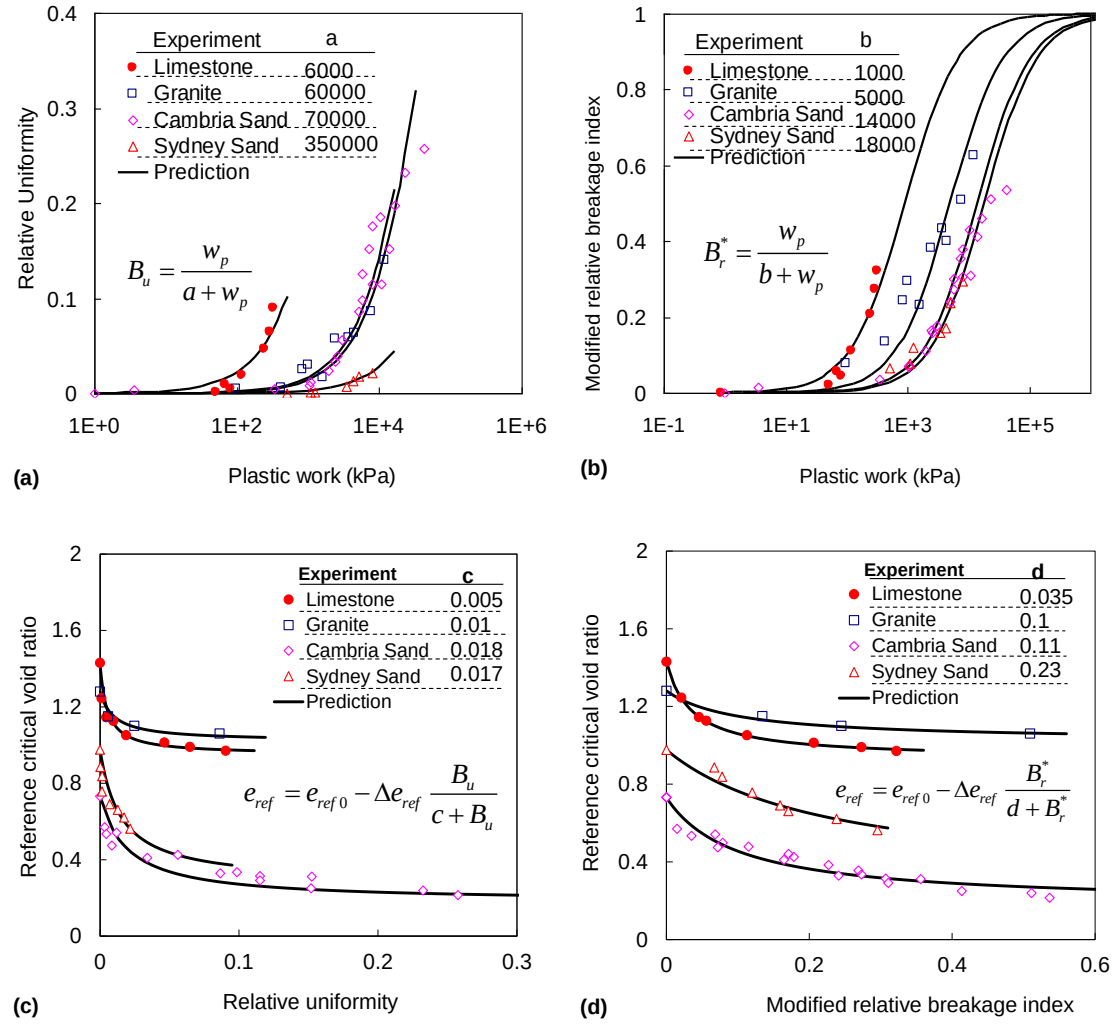

759
760
761 **Fig. 13.** (a) Relative uniformity versus plastic work, (b) Modified relative breakage index versus

plastic work, (c) Reference critical void ratio versus relative uniformity, (d) Reference critical void ratio versus modified relative breakage index.

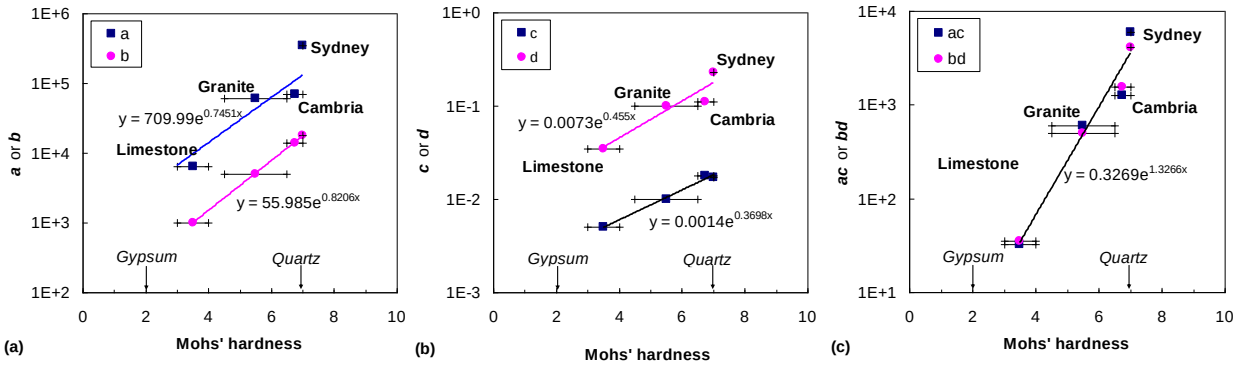

Fig. 14. (a) *a* and *b* values versus Mohs' hardness of materials, (b) *c* and *d* values versus Mohs' hardness of materials, (d) *ac* and *bd* values versus Mohs' hardness of materials.